# Elastic scattering cross sections for the $p+$He system in the energy region of 1.4–24 MeV

A. Nurmela,[a] E. Rauhala, and J. Räisänen
*Department of Physics, Accelerator Laboratory, P.O. Box 43, FIN-00014 University of Helsinki, Finland*

(Received 7 April 1997; accepted for publication 4 June 1997)

The elastic scattering cross sections for proton scattering from $^4$He were determined in the proton energy region of 1.4–6.0 MeV. The measurements were performed at laboratory angles of 110°–170° for proton energies of 1.4–2.7 MeV and at angles of 140° and 170° for proton energies of 2.7–6.0 MeV. The scattering cross sections for $^1$H recoils by $^4$He ion bombardment for helium energies of 5.6–24 MeV at recoil angles of 4°–28° were calculated by kinematically reversing the reaction. The helium targets were prepared by implanting 60 keV $^4$He ions into thin tantalum foils. The helium concentration was determined by transmission elastic recoil detection analysis employing 10 MeV $^{28}$Si ions. The obtained cross section data are compared with the available literature values. Differences up to 10% are found in the values at the cross section curve maximum in comparison to earlier data. © *1997 American Institute of Physics.* [S0021-8979(97)08917-2]

## I. INTRODUCTION

Elemental analysis of helium has gained increased interest, e.g., due to its presence in materials of future fusion reactors,[1] due to novel He-implantation applications[2,3] and the use of He-implantation in the production of optical waveguides.[4,5] A wide selection of analytical techniques exist for microanalysis of helium.[1] Depth profiling of helium can be also realized by several methods based on MeV ion beams. Proton elastic scattering (PES) is a basic method for such analyses.[6] Previously we have applied the proton scattering technique successfully for determination of helium range profiles in compound semiconductors.[7,8]

Hydrogen has in many cases significant effects on the physical, chemical, and electrical properties of materials. It is also a common contaminant element and its analysis with good sensitivity by most routine analytical methods is difficult. The analysis of hydrogen by $^4$He ion elastic recoil detection (ERD) spectrometry is a frequently applied technique for profiling hydrogen in various materials.[9,10]

Deduction of accurate absolute concentration values by the ion beam methods, however, relies on proper elastic scattering cross sections. In case of $^4\mathrm{He}(p,p)^4\mathrm{He}$ scattering several cross section studies have been reported in the literature.[11–15] In these results differences of about 10% occur in the broad maximum of the cross section curve. Furthermore, consistent data have been obtained only for limited scattering angles. No measured data for the $p(^4\mathrm{He},p)^4\mathrm{He}$ recoil scattering cross sections can be found in the literature in the present energy region of $E_{\mathrm{He}}=5.6$–24 MeV.

The purpose of the present work is to provide a consistent set of accurate cross section data for hydrogen, and helium profiling by PES and ERD in the relevant energy regions at several scattering or recoil angles and to fix the values at the cross section curve maximum. For helium profiling by PES the elastic scattering cross sections are measured, and for hydrogen profiling by transmission mode ERD the cross sections are obtained by kinematically reversing the scattering reaction. Implanted helium targets instead of gas targets are employed here for the first time.

## II. EXPERIMENTAL METHODS

### A. Experimental apparatus

The scattering cross section measurements were carried out using proton beams in the energy region of 1.4–2.7 MeV obtained from the 2.5 MV Van de Graaff accelerator of the laboratory. At energies above 2.7 MeV and for obtaining the 10 MeV $^{28}$Si beam the laboratory's 5 MV EGP-10-II tandem accelerator was utilized. The energy calibration of the beam-analyzing magnets was based on the resonances at 991.9 and 1799.8 keV of the reaction $^{27}\mathrm{Al}(p,\gamma)^{28}\mathrm{Si}$.

Scattering chambers 0.7 m diam equipped with standard backscattering apparatus were employed. Several ion implanted silicon detectors were placed at laboratory angles of 110°–170°. At energies below 2.7 MeV three detectors (25 mm$^2$, 100 $\mu$m) and at higher energies two (25 mm$^2$, 300 $\mu$m) detectors were used. The solid acceptance angles of the detectors were 3.10 msr. The beam collimation and detector positions confined the angular resolution to $\pm 2.0°$. The energy resolution of the detection system was typically 12 keV for protons.

### B. Sample preparation

The helium targets were prepared by implanting 60 keV $^4$He ions in 1.50-$\mu$m-thick tantalum foils. The resulting helium depth distribution has a mean range of 180 nm and a width of 85 nm (standard deviation) as calculated by Monte Carlo simulation.[16]

The reason for the choice of a thin self supporting foil of a heavy material for the implantations is to obtain as low background as possible, in the spectrum region including the proton backscattering signal from helium. Tantalum was chosen for the backing material since it is known,[17] that helium does not migrate in tantalum even when annealed for 30 min at 1070 K. In addition, the cross section measurements were repeated at regular intervals at reference energies to

[a]Corresponding author. Electronic mail: Arto.Nurmela@Helsinki.Fi

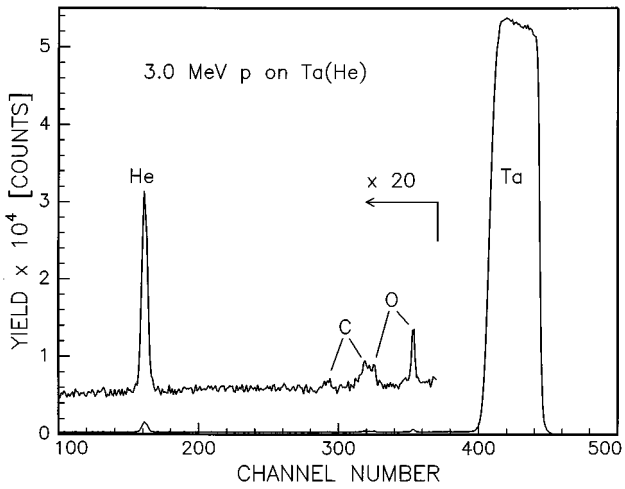


FIG. 1. Backscattering spectrum for 3.0 MeV protons incident on a tantalum foil implanted with $1.6\times10^{17}$ $^4$He ions/cm$^2$. The scattering angle is 170°. The scattering yield below channel number 370 has been multiplied by 20 for clarity. The peaks denoted as O and C originate from carbon and oxygen impurities at Ta surfaces.

check for possible changes in the sample composition. No changes, however, were observed. In our recent study, proton scattering from tantalum has been observed to be pure Rutherford in the present energy region $\leqslant$6.0 MeV.[18] A backscattering spectrum for protons incident on the Ta(He) sample is shown in Fig. 1. The signal from tantalum in the spectrum may be used as an internal reference for the proton-beam dose.

Four different $^4$He doses, $1.0\times10^{16}$, $5.0\times10^{16}$, $1.0\times10^{17}$, and $2.0\times10^{17}$ ions/cm$^2$ were implanted to investigate the correspondence between the helium content in the foil and the implanted helium dose, and the consistency of the implantation results. The dose values are based on an up-to-date current integration procedure with an electron suppression system. Figure 2 shows the accurate linear dependence between the scattering yield and the integrated dose, indicating a good relative accuracy and that all the doses fall below the saturation level of helium in Ta. The sample with the highest implantation dose was employed in the cross section measurements.

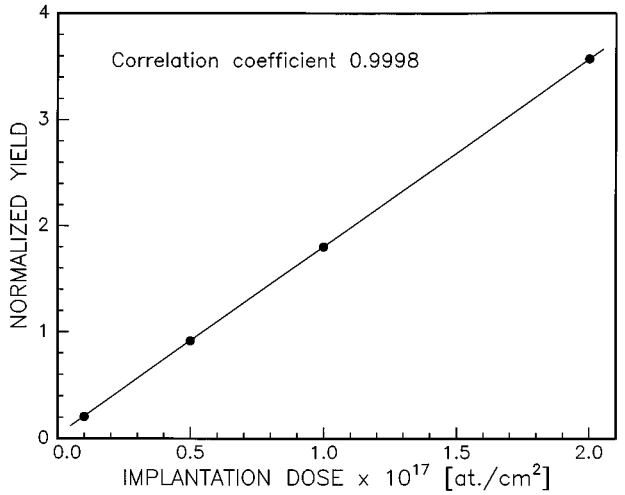


FIG. 2. Normalized signal peak area for proton scattering from helium at 2.7 MeV as a function of implanted $^4$He ion dose. A linear least squares fit to the data points is also shown.

The absolute helium content in the sample implanted with the highest dose was determined by 10 MeV $^{28}$Si ion transmission ERD analysis. This was done by simultaneously employing two detectors, one to detect the $^4$He recoils at a recoil angle of 10° and another to measure the backscattering yield of the incident $^{28}$Si particles at a scattering angle of 170°. The height of the backscattering signal of Ta was then used for the absolute calibration of the ERD measurements. A 2.5-$\mu$m-thick Havar absorber foil was used to stop the incident particles from entering the transmission detector. The energy $E_{\mathrm{Si}}=10$ MeV utilized for the recoil process $^4$He($^{28}$Si, $^4$He) $^{28}$Si is well below the non-Rutherford threshold, as can be verified by analysing the corresponding scattering process $^{28}$Si($^4$He, $^4$He)$^{28}$Si. The stopping powers from Ref. 16 were used in the calculations.

An areal density of $(1.60\pm0.08)\times10^{17}$ ions/cm$^2$ was obtained for helium. This value may be compared with dose based on current integration when taking into account the fraction of the reflected $^4$He ions during the implantation. By Monte Carlo simulations,[16] the fraction of the $^4$He ions backscattered from the Ta foil is calculated as 11%. This is in agreement with the helium content determined via ERD within experimental uncertainty.

A noteworthy difference in the present study in comparison to the previous elastic scattering cross section studies reported in Refs. 11–15 is the use of implanted solid helium targets. By this choice and by using the Ta signal as an internal dose reference in the cross section measurements, we eliminate the need for accurate current integration of the bombarding proton beam.

## III. DATA ANALYSIS

The ratio $(Nt)_{\mathrm{Ta}}/(Nt)_{\mathrm{He}}$ ($N$=atom density, $t$=layer thickness) was determined using the areal density value for $(Nt)_{\mathrm{He}}$ from ERD measurements and measuring $(Nt)_{\mathrm{Ta}}$ by 2.7 MeV proton backscattering. The elastic scattering cross sections in the laboratory coordinates were then calculated from:

$$\sigma_{\mathrm{He}}(E)=\sigma_{\mathrm{Ta,Ruth}}(E_2)A_{\mathrm{He}}(Nt)_{\mathrm{Ta}}/A_{\mathrm{Ta}}(Nt)_{\mathrm{He}},$$

where $E=E_0-\Delta E_{\mathrm{Ta(1)}}-\Delta E_{\mathrm{He}}/2$ and $E_2=E_0-\Delta E_{\mathrm{Ta(2)}}/2$. The symbol $E_0$ represents the incident proton energy, $\Delta E_{\mathrm{Ta(1)}}$, $\Delta E_{\mathrm{He}}$, and $\Delta E_{\mathrm{Ta(2)}}$ denote the energy-dependent proton energy losses in the tantalum layer in front of the $^4$He implanted layer, the $^4$He implanted layer and the 1.50 $\mu$m tantalum foil, respectively. The stopping powers from Ref. 16 were used in the energy loss calculations. The cross section $\sigma_{\mathrm{Ta,Ruth}}(E_2)$ is the calculated proton Rutherford scattering cross section of tantalum, corrected for electronic screening.[19] The signal peak area ratios $A_{\mathrm{He}}/A_{\mathrm{Ta}}$ were determined from the measured spectra. This procedure of obtaining the cross section values has been used also in our previous cross section studies.[20–24]

To calculate the cross sections for the kinematically reversed recoil process $p(^4\mathrm{He},p)^4\mathrm{He}$, the identity of the direct

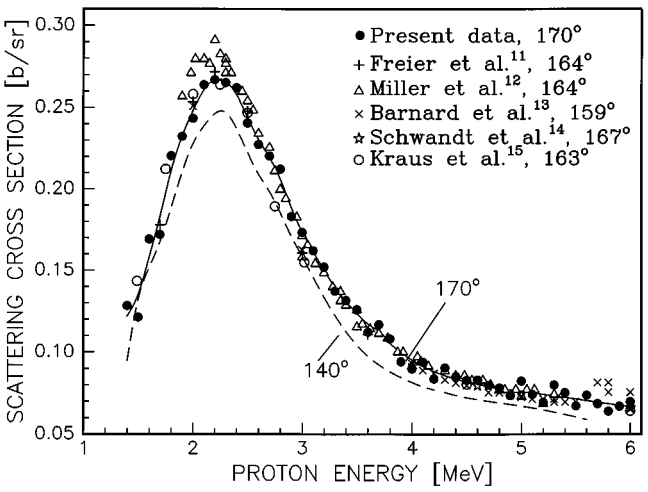


FIG. 3. The present $^4$He$(p,p)^4$He elastic scattering cross sections at the scattering angle of 170° as a function of proton energy and a comparison to earlier data published near 170°. A smoothened curve is drawn through the present data points to guide the eye. A similar curve for the present data taken at 140° is illustrated with the data points omitted for clarity.

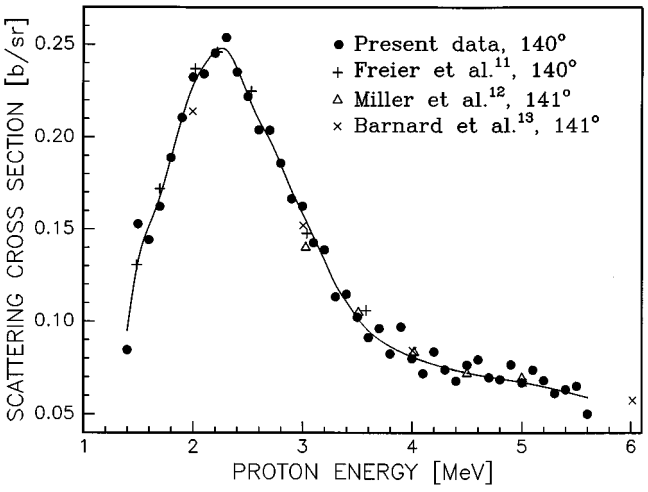


FIG. 4. The present $^4$He$(p,p)^4$He elastic scattering cross sections at the scattering angle of 140° as a function of proton energy and a comparison to earlier data published near 140°. A smoothened curve is drawn through the present data points to guide the eye.

and inverse processes in the center of mass frame of reference was utilized. This leads to recoil cross sections obtained by scaling from the direct scattering cross section curves for each angle and energy. The experimental proton energies $E_H = 1.4–6.0$ MeV and scattering angles of 110°–170° of the direct process correspond to calculated $^4$He ion energies $E_{\mathrm{He}} = 5.6–24.0$ MeV, and recoil angles of 15°–4° of the reversed process. The recoil angles are the angles between the direction of the recoiling $^1$H and the direction defined by the incident $^4$He beam direction behind the sample foil. All values given in the present study refer to the laboratory frame of reference.

## IV. RESULTS AND DISCUSSION

The excitation functions for the direct scattering process $^4$He$(p,p)^4$He at angles of 170° and 140° are presented in Figs. 3 and 4, and given in Table I. The curves increase abruptly and after reaching a broad maximum at about $E_H = 2.2$ MeV, decrease with increasing energy. At the maximum, the cross section enhancement ratio (cross section/Rutherford cross section) is 265 for the scattering angle of 170°. With increasing energy, this ratio increases to 540 at $E_H = 6.0$ MeV. As may be noted the cross sections are systematically lower for the smaller scattering angle. Cross sections for the kinematically reversed recoil reaction $p(^4\mathrm{He},p)^4$He are shown in Fig. 5 and tabulated in Table II for $^4$He ion energies of 5.6–24 MeV and recoil angles of 4° and 15°. The enhancement ratios are 265 and 215 at the cross section maxima at $E_{\mathrm{He}} = 8.8$ MeV and 465 and 310 at $E_{\mathrm{He}} = 22$ MeV for the recoil angles of 4° and 15°, respectively. The data presented are useful for hydrogen profiling by $^4$He in the transmission mode of ERD spectrometry.

The angular dependence of the backscattering cross sections together with the values for the reversed recoil reaction are given in Fig. 6 for various ion energies. In all cases smooth cross section behavior with no broad resonancelike structures is observed.

The uncertainty associated with the absolute helium content is 5%, which comprises the uncertainties arising from the ERD measurements by $^{28}$Si ions. The uncertainties in the cross section values increase from 6% at the low energy end to 7% at the high energy end. These uncertainties result from statistical errors and background subtraction uncertainties in the helium peak area determination and from the uncertainty in the helium content. When comparing the cross sections taken at different energies, these relative values are more accurate with an estimated inaccuracy below 3%.

The possible effect of multiple scattering was investigated by taking proton backscattering spectra also from the backside of the $^4$He implanted Ta foil. By this arrangement the mean depth of the helium distribution in the Ta foil increased from 180 to 1320 nm. The ratio of the signal areas $A_{\mathrm{Ta}}/A_{\mathrm{He}}$, however, was found invariant after appropriate energy loss corrections within the experimental accuracy of 2%, confirming the insignificance of the multiple scattering contribution.

The present values may be compared with the elastic scattering cross sections found in the literature. The comparison for $^4$He$(p,p)^4$He is presented in Figs. 3 and 4. Some of the earlier data points plotted have been extracted from published graphs. The scattering angles in the earlier studies included in Figs. 3 and 4 differ slightly from 170° or 140°, but this effect is negligible as may be concluded from the curves for angles of 140° and 170° of Fig. 3. When taking into account the fact that the relative cross sections of this study are more accurate (uncertainty less than 3%), than the absolute values and that all the data sets at higher energies are in good agreement, differences may be noted around the curve maximum, where the data of Refs. 11–15 taken near 170° differ most from each other. Our cross section values fall about 10% below those of Miller *et al.*[12] (quoted uncer-

TABLE I. Elastic scattering cross sections for the $^4$He $(p,p)$ $^4$He scattering process at scattering angles of 140° and 170° as a function of proton energy. All values refer to the laboratory frame of reference. The uncertainties of the cross section data are 6% below and 7% above 4.5 MeV.

| | Cross section [b/sr] | |
|---|---|---|
| Energy [MeV] | 140° | 170° |
| 1.4 | 0.085 | 0.128 |
| 1.5 | 0.153 | 0.121 |
| 1.6 | 0.144 | 0.169 |
| 1.7 | 0.162 | 0.172 |
| 1.8 | 0.189 | 0.220 |
| 1.9 | 0.210 | 0.232 |
| 2.0 | 0.232 | 0.243 |
| 2.1 | 0.234 | 0.264 |
| 2.2 | 0.245 | 0.267 |
| 2.3 | 0.254 | 0.265 |
| 2.4 | 0.235 | 0.262 |
| 2.5 | 0.222 | 0.241 |
| 2.6 | 0.204 | 0.227 |
| 2.7 | 0.204 | 0.220 |
| 2.8 | 0.186 | 0.212 |
| 2.9 | 0.167 | 0.183 |
| 3.0 | 0.163 | 0.173 |
| 3.1 | 0.143 | 0.162 |
| 3.2 | 0.139 | 0.152 |
| 3.3 | 0.113 | 0.137 |
| 3.4 | 0.115 | 0.132 |
| 3.5 | 0.102 | 0.126 |
| 3.6 | 0.091 | 0.112 |
| 3.7 | 0.096 | 0.117 |
| 3.8 | 0.082 | 0.108 |
| 3.9 | 0.097 | 0.094 |
| 4.0 | 0.080 | 0.090 |
| 4.1 | 0.072 | 0.094 |
| 4.2 | 0.084 | 0.084 |
| 4.3 | 0.074 | 0.090 |
| 4.4 | 0.068 | 0.085 |
| 4.5 | 0.076 | 0.083 |
| 4.6 | 0.079 | 0.083 |
| 4.7 | 0.070 | 0.080 |
| 4.8 | 0.069 | 0.078 |
| 4.9 | 0.077 | 0.074 |
| 5.0 | 0.067 | 0.082 |
| 5.1 | 0.074 | 0.074 |
| 5.2 | 0.068 | 0.069 |
| 5.3 | 0.061 | 0.080 |
| 5.4 | 0.063 | 0.075 |
| 5.5 | 0.065 | 0.067 |
| 5.6 | 0.050 | 0.074 |
| 5.7 | | 0.069 |
| 5.8 | | 0.064 |
| 5.9 | | 0.067 |
| 6.0 | | 0.070 |

tainty 2.6%) and 2% below those of Freier *et al.*[11] (uncertainty 3%), but are in agreement with most data points of Kraus *et al.*[15] (uncertainty 6%). For 140°, data from Refs. 11–13 are found around the cross section maximum, with reasonable agreement with the present data. We believe that our systematic data represent more accurately the elastic scattering cross sections around the broad maximum than the data published earlier.

Below $E_{\mathrm{He}}=4.5$ MeV measured data on the elastic scattering cross sections for the recoil reaction $p(^4\mathrm{He},p)^4\mathrm{He}$ at various recoil angles of 20°–42° have been published.[25–29] These data show smooth, slowly decreasing cross sections with increasing energy up to 3.0 MeV. At this energy the cross sections start to slowly increase. At 4.5 MeV a cross section of about 0.35 b/sr at 30° was reported.[25] Cross sections up to 8.0 MeV have been deduced,[28,30,31] by kinematically reversing the calculated $^4\mathrm{He}(p,p)^4\mathrm{He}$ scattering data based on phase shift analysis. These data, given for slightly different recoil angles are in qualitative agreement with the present results.

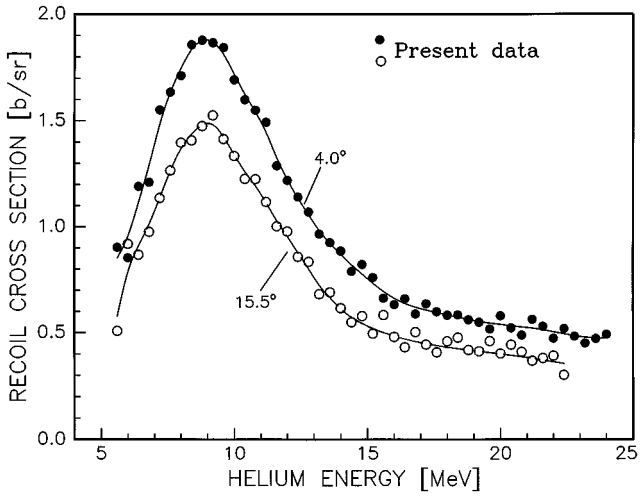


FIG. 5. Elastic scattering cross sections for the $p(^4\mathrm{He},p)^4\mathrm{He}$ recoil process at recoil angles of 4.0° and 15.5° as a function of $^4$He ion energy. The curves as in Fig. 4.

The glancing mode ERD enhancement ratios at low He ion energies are found significantly smaller than the present transmission mode cross sections at high energies. For example, the cross section enhancement ratio increases from about 2 to 3 at $E_{\mathrm{He}}=2.8$ MeV (Ref. 29) with decreasing recoil angles from 35° to 20°. These enhancement ratios can be compared to the ratios of 265 and 540 obtained in the present study for $E_{\mathrm{He}}=8.8$ and 24 MeV at the recoil angle of 4°.

From Figs. 3 to 6 the optimum geometry and projectile energy as regards the scattering cross sections both in PES and ERD spectrometries may be deduced. High absolute cross sections near the cross section curve maximum around $E_H=2.2$ MeV (PES) and at $E_{\mathrm{He}}=8.8$ MeV (ERD) result in good absolute sensitivity. However, better signal to background ratio may be obtained at high values of the enhancement ratio. These values are found at significantly higher incident ion energies, close to the high energy limits $E_H=6.0$ MeV (PES) and $E_{\mathrm{He}}=24.0$ MeV (ERD) of the present measurements. In the proton backscattering geometry, larger scattering angles produce higher absolute cross sections. This circumstance is reversed for the recoil geometry, where smaller recoil angles render higher elastic scattering cross sections.

## V. CONCLUSIONS

The cross sections for the $^4\mathrm{He}(p,p)^4\mathrm{He}$ scattering in the energy region of $E_p=1.4-6.0$ MeV, together with the data

TABLE II. Elastic scattering cross sections for the $p(^4\mathrm{He},p)^4\mathrm{He}$ recoil process at recoil angles of 4.0° and 15.5° as a function of $^4$He ion energy. All values refer to the laboratory frame of reference. The uncertainties of the cross section data are 6% below and 7% above 18.0 MeV.

| | Cross section [b/sr] | |
|---|---|---|
| Energy [MeV] | 4.0° | 15.5° |
| 5.6 | 0.903 | 0.509 |
| 6.0 | 0.853 | 0.919 |
| 6.4 | 1.190 | 0.867 |
| 6.8 | 1.210 | 0.976 |
| 7.2 | 1.551 | 1.136 |
| 7.6 | 1.635 | 1.266 |
| 8.0 | 1.712 | 1.398 |
| 8.4 | 1.857 | 1.408 |
| 8.8 | 1.878 | 1.476 |
| 9.2 | 1.867 | 1.526 |
| 9.6 | 1.844 | 1.415 |
| 10.0 | 1.693 | 1.335 |
| 10.4 | 1.599 | 1.227 |
| 10.8 | 1.550 | 1.226 |
| 11.2 | 1.493 | 1.118 |
| 11.6 | 1.288 | 1.002 |
| 12.0 | 1.219 | 0.978 |
| 12.4 | 1.141 | 0.858 |
| 12.8 | 1.070 | 0.835 |
| 13.2 | 0.965 | 0.682 |
| 13.6 | 0.926 | 0.690 |
| 14.0 | 0.885 | 0.615 |
| 14.4 | 0.789 | 0.549 |
| 14.8 | 0.822 | 0.578 |
| 15.2 | 0.760 | 0.496 |
| 15.6 | 0.662 | 0.583 |
| 16.0 | 0.632 | 0.480 |
| 16.4 | 0.660 | 0.432 |
| 16.8 | 0.588 | 0.503 |
| 17.2 | 0.636 | 0.445 |
| 17.6 | 0.599 | 0.408 |
| 18.0 | 0.583 | 0.460 |
| 18.4 | 0.584 | 0.477 |
| 18.8 | 0.561 | 0.419 |
| 19.2 | 0.549 | 0.413 |
| 19.6 | 0.517 | 0.461 |
| 20.0 | 0.580 | 0.402 |
| 20.4 | 0.522 | 0.444 |
| 20.8 | 0.488 | 0.410 |
| 21.2 | 0.563 | 0.368 |
| 21.6 | 0.529 | 0.380 |
| 22.0 | 0.474 | 0.391 |
| 22.4 | 0.519 | 0.301 |
| 22.8 | 0.483 | |
| 23.2 | 0.451 | |
| 23.6 | 0.472 | |
| 24.0 | 0.491 | |

for the kinematically reversed reaction $p(^4\mathrm{He},p)^4\mathrm{He}$ for $E_{\mathrm{He}}=5.6-24$ MeV have been determined with good relative accuracy. A cross section enhancement of 540 was obtained for $^4\mathrm{He}(p,p)^4\mathrm{He}$ at $E_p=6.0$ MeV (scattering angle 170°) and for $p(^4\mathrm{He},p)^4\mathrm{He}$ at $E_{\mathrm{He}}=24$ MeV (recoil angle 4°). The values in the energy region showing the cross section curve maximum have been established consistently. This has a significant effect on accurate helium and hydrogen concentration profile determinations.

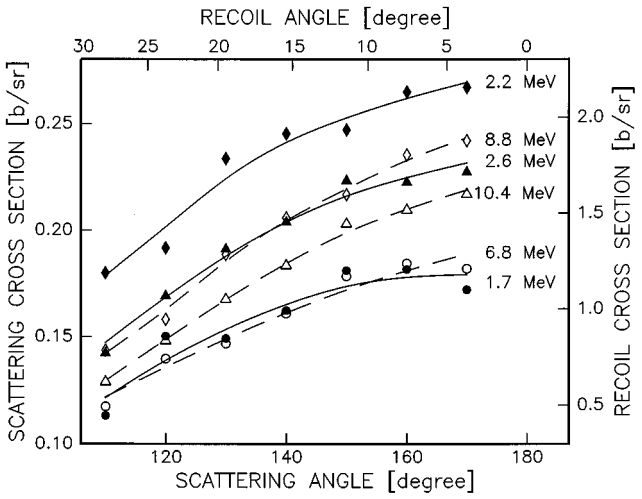


FIG. 6. Scattering angular distributions for the system $p+^4\mathrm{He}$. The solid symbols and curves represent the $^4\mathrm{He}(p,p)^4\mathrm{He}$ scattering process at proton energies of 1.7, 2.2, and 2.6 MeV (left and lower axes), the open symbols and dashed curves correspond to the $p(^4\mathrm{He},p)^4\mathrm{He}$ recoil process at $^4$He ion energies of 6.8, 8.8, and 10.4 MeV (right and upper axes).

Differences up to 10% in the cross sections were found when compared to previous studies presented in the literature. These differences may be partly due to problems with current integration, and anomalous behavior of the gas targets used in the previous studies. In the present work implanted solid targets were used for the first time. The obtained systematic and accurate cross section values will be employed in our future studies of helium concentration distributions in metals and compound semiconductors.

## ACKNOWLEDGMENT

This work was supported in part, by the Academy of Finland within the framework of EPIMATTER project.

[1] F. Pászti, Nucl. Instrum. Methods Phys. Res. B **66**, 83 (1992).
[2] M. Bruel, Nucl. Instrum. Methods Phys. Res. B **108**, 313 (1996).
[3] C. C. Griffioen, J. H. Evans, P. C. de Jong, and A. Van Veen, Nucl. Instrum. Methods Phys. Res. B **27**, 417 (1987).
[4] Y. Avrahami and E. Zolotoyabko, Nucl. Instrum. Methods Phys. Res. B **120**, 84 (1996).
[5] P. Bindner, A. Boudrioua, J. C. Loulergue, and P. Moretti, Nucl. Instrum. Methods Phys. Res. B **120**, 88 (1996).
[6] E. Rauhala, in *Elemental Analysis by Particle Accelerators*, edited by Z. B. Alfassi and M. Peisach (CRC, Boca Raton, 1992), pp. 179–241.
[7] E. Rauhala and J. Räisänen, Nucl. Instrum. Methods Phys. Res. B **94**, 245 (1994).
[8] K. Väkeväinen, M. Rajatora, T. Ahlgren, E. Rauhala, and J. Räisänen, Appl. Surf. Sci. (in print).
[9] W. A. Lanford, Nucl. Instrum. Methods Phys. Res. B **66**, 65 (1992).
[10] F. Pászti, E. Szilagyi, and E. Kotai, Nucl. Instrum. Methods Phys. Res. B **54**, 507 (1991).
[11] G. Freier, E. Lampi, W. Sleator, and J. H. Williams, Phys. Rev. **75**, 1345 (1949).
[12] P. D. Miller and G. C. Phillips, Phys. Rev. **112**, 2043 (1958).
[13] A. C. L. Barnard, C. M. Jones, and J. L. Weil, Nucl. Phys. **50**, 604 (1964).
[14] P. Schwandt, T. B. Clegg, and W. Haeberli, Nucl. Phys. A **163**, 432 (1971).
[15] L. Kraus and I. Link, Nucl. Phys. A **224**, 45 (1974).
[16] J. F. Ziegler, SRIM-96 computer code (private communication).
[17] P. Haussalo, J. Keinonen, U.-M. Jäske, and J. Sievinen, J. Appl. Phys. **75**, 7770 (1994).

[18] V. Zazubovich, A. Nurmela, E. Rauhala, R. Lappalainen, and J. Räisänen (unpublished).
[19] H. H. Andersen, F. Besenbacher, P. Loftager, and W. Möller, Phys. Rev. A **21**, 1891 (1980).
[20] E. Rauhala and J. Räisänen, Nucl. Instrum. Methods Phys. Res. B **35**, 7 (1988).
[21] J. Räisänen and E. Rauhala, Nucl. Instrum. Methods Phys. Res. B **73**, 439 (1993).
[22] E. Rauhala and J. Räisänen, J. Appl. Phys. **75**, 642 (1994).
[23] J. Räisänen, E. Rauhala, J. M. Knox, and J. F. Harmon, J. Appl. Phys. **75**, 3273 (1994).
[24] J. Räisänen and E. Rauhala, J. Appl. Phys. **77**, 1762 (1995).
[25] D. C. Ingram, A. W. McCormick, P. P. Pronko, J. D. Carlson, and J. A. Woollam, Nucl. Instrum. Methods Phys. Res. B **6**, 430 (1985).
[26] S. Nagata, S. Yamaguchi, Y. Hou, N. Sugiyama, and K. Kamada, Nucl. Instrum. Methods Phys. Res. B **6**, 533 (1985).
[27] F. Pászti, E. Kotai, G. Mezey, A. Manuaba, L. Pocs, D. Hillebrandt, and H. Strunsny, Nucl. Instrum. Methods Phys. Res. B **15**, 486 (1986).
[28] J. Tirira, P. Trocellier, J. P. Frontier, and P. Trouslard, Nucl. Instrum. Methods Phys. Res. B **45**, 203 (1990).
[29] J. E. E. Baglin, A. J. Kellock, M. A. Crockett, and A. H. Shih, Nucl. Instrum. Methods Phys. Res. B **64**, 469 (1992).
[30] L. S. Wielunski, R. E. Benenson, and W. A. Lanford, Nucl. Instrum. Methods Phys. Res. **218**, 120 (1983).
[31] Y. Wang, J. Chen, and F. Huang, Nucl. Instrum. Methods Phys. Res. B **17**, 11 (1986).